ISSN 1392–1320 MATERIALS SCIENCE (MEDŽIAGOTYRA). Vol. XX, No. X. 2022

High-temperature Oxidation Properties of TiC-reinforced Mo Matrix Composites with Cr Element Added

Hongtao LI [1], Renheng HAN [1], Fangchao PENG [1], Hongliang YIN [1], Ming TANG [1], Hexin ZHANG [1, 2]*, Chengzhi ZHAO [1, 2]

[1] *College of Materials Science and Chemical Engineering, Harbin Engineering University, No. 145 Nantong Avenue, Harbin, Heilongjiang, 150001, China*
[2] *Key Laboratory of Superlight Materials and Surface Technology of Ministry of Education, Harbin Engineering University, No. 145 Nantong Avenue, Harbin, Heilongjiang, 150001, China*

crossref http://dx.doi.org/10.5755/j02.ms.30338

Received XX June 201X; accepted XX December 201X

This work studied Mo-TiC-xCr (x = 0.0, 0.5, 1.0 wt.%) matrix composites with different component gradients prepared by Spark Plasma Sintering (SPS). The high-temperature oxidation test was conducted at 1200 ℃ in the atmosphere to study the influence of Cr on the high-temperature oxidation behavior of TiC-reinforced Mo matrix composites. The phase composition and morphology of the oxide film were analyzed using X-ray diffraction (XRD), scanning electron microscopy (SEM), and energy dispersive spectroscopy (EDS), and the goal was to determine the effect of the Cr content on the high-temperature oxidation properties of the Mo-TiC-xCr (x = 0.0, 0.5, 1.0 wt.%) matrix composites. The results showed that with increasing oxidation time, the oxide film on the surface of Mo alloy will crack and fall off easily, and the porosity gradually increases. Oxygen underwent vigorous oxidation through the pores and the inside of the matrix, and a protective MoO_2 internal oxide film disappeared. With increasing Cr content, the high-temperature oxidation performance of the Mo alloy improved, the thickness of the oxide film decreased, warping of the surface oxide film was inhibited, the porosity decreased, and volatilization of MoO_3 was inhibited. After oxidation, the surface oxide film was mainly composed of TiO_2, MoO_3, Cr_2O_3 and $Cr_2(MoO_4)_3$ phases. The TiC particles dispersed in the matrix were oxidized to TiO_2 to inhibit the oxidation of the alloy. The Cr formed a protective oxidation film of Cr_2O_3, which effectively reduced the porosity and delayed the volatilization of the MoO_3, thus improving its oxidation performance.
Keywords: high-temperature oxidation, composite materials, TiC, Mo alloy.

1. INTRODUCTION

Modern industry is increasing the requirements for structural materials used in high-temperature environments [1 – 3]. As a refractory metal, molybdenum has a high melting point (2620 ℃), a high elastic modulus (320 – 350 GPa), high wear resistance, good electrical and thermal conductivity and strong corrosion resistance, making it an excellent high-temperature material [4]. At present, molybdenum and its alloys have been widely used in steel, the metallurgy industry, machinery components, the chemical industry, and the aerospace industry, to name a few [5 – 8].

By using carbide as the enhancement phase, the discharge plasma sintering method (spark plasma sintering, SPS) preparation of molybdenum alloys has emerged in recent years as a rapid sintering process [9 – 11]. The sintering temperature of this method is lower than that of the traditional process, the sintering time is shorter, the operation is simple, and a fine grain structure can be obtained [12]. By adding Ti, Zr, Hf and other active elements that react with C to produce refractory carbides (TiC, ZrC, and HfC, respectively), the strength and toughness of the material can be significantly improved [13]. Dispersed particles appear in the grain boundaries of molybdenum alloys in the form of Ti (O_x, C) or Hf (O_x, C) compounds, which effectively prevent grain growth and thus improve the high-temperature properties of molybdenum alloys [14, 15]. However, molybdenum and molybdenum industrial alloys undergo destructive oxidation above 700 ℃, severely limiting their potential as heat-resistant structural materials. Therefore, it is necessary to improve the high-temperature oxidation performance of molybdenum alloys by improving the alloy composition [16, 17]. Since Cr only produces a single oxide, Cr_2O_3, the oxidation resistance of the material can be improved by forming a Cr_2O_3 film [18]. At the same time, the addition of Cr does not significantly affect the properties of molybdenum and molybdenum alloys [19, 20].

In this paper, a new TiC-reinforced molybdenum-based composite was prepared by adding Cr and using the SPS method Improving the oxidation resistance of the material was explored based on the premise of not significantly changing the microstructure of the material. The microstructure and oxidation mechanism under different temperatures and oxidation times were studied after adding Cr. The oxidation resistance of the new TiC-reinforced molybdenum-based composites was evaluated by analyzing the oxidation kinetics curves of the new alloys, the surface and cross-section morphologies, and the composition of the oxide. This provides a reference for further research on the oxidation resistance of molybdenum-based alloys.

* Corresponding author. Tel.: +86-18645106806.
E-mail address: *zhanghx@hrbeu.edu.cn* (H. Zhang)

2. MATERIALS AND METHODS

2.1. Materials

The test components comprised Mo-5TiC-xCr (x = 0.0, 0.5 and 1.0 wt.%). A ball mill process was used to mix the elemental powders. The parameters of the ball mill were as follows: the ball material ratio was 2:1, the ball mill time was 5 h, the rotation speed was 200/rpm, and the ball mill tank was filled with argon as a protective gas. The ball mill process was as follows: after dry mixing, the powder was compacted at the bottom of the ball mill tank, and the balls floated on it. Then, ethanol was added as the ball grinding medium and mixing continued. The powder was then treated in a vacuum drying box at 100 ℃ for 1 h and sifted into a 200 mesh sieve. Then, an analytical balance was used, to measure 300 g of powder that was then placed in the Ø40 graphite mold. Graphite paper was attached to the inside of the mold and the contact surface between the head and the powder before charging. Then, the mold was placed into the SPS furnace. The temperature was increased from room temperature to 1700 ℃ at a speed of 100 K/min, and the pressure was increased from 5 MPa to 30 MPa. Then, the temperature was held for 9 min and finally cooled with the furnace.

2.2. Methods

In this experiment, a high temperature resistance furnace (Model SM-28-10) was used for the high temperature oxidation test. The samples with different components were cut into rectangular blocks with dimensions of 10 mm × 20 mm × 1.5 mm. After the material was ground and polished, it was ultrasonically cleaned with ethanol and dried for use. The cyclic oxidation test method and weight loss method were used to measure the high-temperature oxidation kinetics curve of the sample under an atmospheric environment at 1200 ℃. The oxidation times were 5 min, 10 min, 20 min, 30 min, 40 min and 60 min. An analytical balance with an accuracy of 0.0001 g was used to weigh the mass change before and after oxidation.

The phase analysis of the materials was performed by X-ray diffraction (XRD) (X Pert Pro) with Cu Kα radiation (λ = 1.5406 Å) and a 2θ range of 10° to 90°. The microstructure observations and composition analysis were conducted by using scanning electron microscopy (SEM) and energy dispersive spectroscopy (EDS) (Quanta 200, FEI Company). Before the analysis, deposition of nonconductive oxides on samples by a sputter coater (Model Bal-TEC SCD005). The voltage of the scanning electron microscope was 15 kV.

3. RESULTS AND DISCUSSION

3.1. Oxidation kinetics at high temperatures

Fig. 1 shows the oxidation kinetics curve for the Mo-TiC-xCr alloy system oxidized in an air environment at 1200 ℃ for 60 min. It can be seen in Fig. 1 that the oxidation kinetics curve of the Mo-TiC-xCr composite system is clearly divided into two stages. The first 20 min is a slow oxidation stage, and the loss of mass due to oxidation is low, which is consistent with a parabolic trend. The last 40 mins is the rapid oxidation stage, and the loss of mass due to oxidation mass is linear. The obvious segmentation of the oxidation kinetics curve is mainly due to the different oxidation mechanisms during the high-temperature oxidation process. During the early stage of oxidation, the experimental material alloy system is protected by the inner oxide film of MoO_2 so that oxygen could not penetrate into the substrate excessively, and the oxide film plays a certain protective role [21]. With increasing oxidation time, the MoO_2 oxide film ruptures after reaching the critical thickness, resulting in a large amount of MoO_3. The sublimation of the MoO_3 causes a large number of holes in the material, and a rapid increase in the mass loss causes a sharp increase in the oxidation rate. The oxidation has the characteristics of autocatalysis, and this is confirmed because the oxidation kinetics curve conforms to the trend for autocatalysis. The introduction of Cr has a certain effect on the oxidation mechanism. As the content of Cr increases, the loss of oxidative mass gradually decreases. Since Cr is easily oxidized to Cr_2O_3 at high temperatures, it has a certain protective effect on the alloy [22].

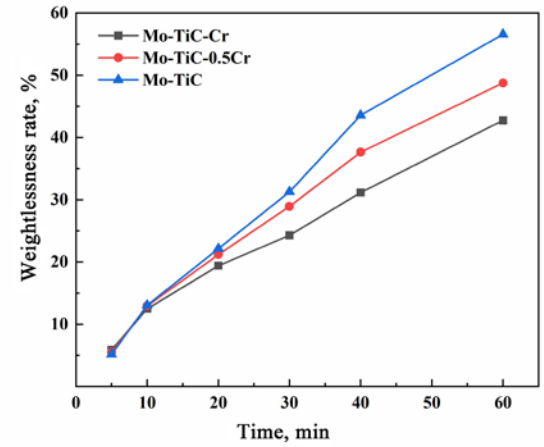

Fig. 1. High-temperature oxide kinetics curve for the Mo-TiC-xCr (x = 0.0, 0.5 and 1.0 wt.%)

3.2. Analysis of high-temperature oxidation products

To investigate the effect of the introduction of Cr on the oxidation products of Mo-TiC-based materials and the types and contents of oxidation products of Mo-TiC-xCr alloy systems at different oxidation times, XRD phase analysis was performed on the corresponding materials. The results are shown in Fig. 2. The oxidation products of the Mo-TiC system are mainly TiO_2, MoO_3, and some very small amounts of unoxidized and dispersed TiC particles. The introduction of Cr, in addition to the abovementioned oxidation products, produces Cr_2O_3 and $Cr_2(MoO_4)_3$. It can also be seen from Fig. 2 that with increasing oxidation time, new oxidation products are formed in the Mo-TiC-xCr alloy system. When the oxidation time is 10 mins, the oxidation surface is mainly composed of TiO_2 and MoO_3, and a small amount of Cr_2O_3 is formed. With increasing oxidation time, TiO_2 still maintained a relatively strong peak, the peak value of Cr oxide also increased accordingly, and the production of $Cr_2(MoO_4)_3$ also gradually increased. Therefore, the main oxidation products of the Mo-TiC-Cr alloy system after

60 min of oxidation are TiO_2, MoO_3, Cr_2O_3 and $Cr_2(MoO_4)_3$.

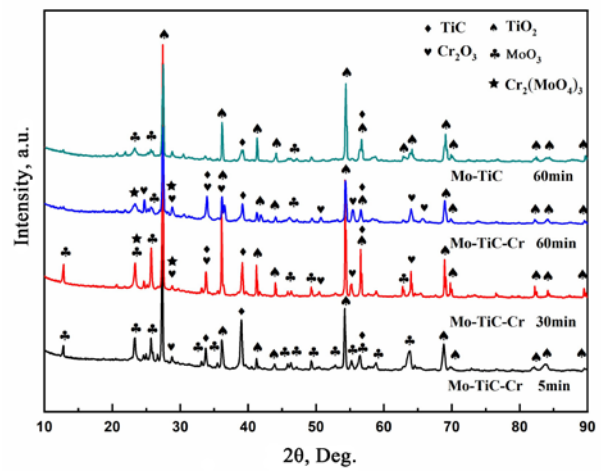

Fig. 2. XRD map of the surface phases on the Mo-TiC-xCr (x = 0.0, 1.0 wt.%)

3.3. Characteristics of the oxidized surface morphology

Fig. 3 shows the micrographs of the oxidized surface morphology of the Mo-TiC-Cr composite material after 10 min, 40 min and 60 min.

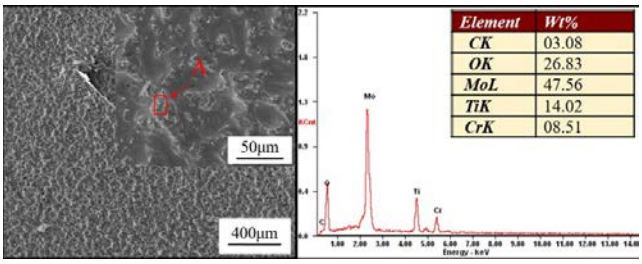

a

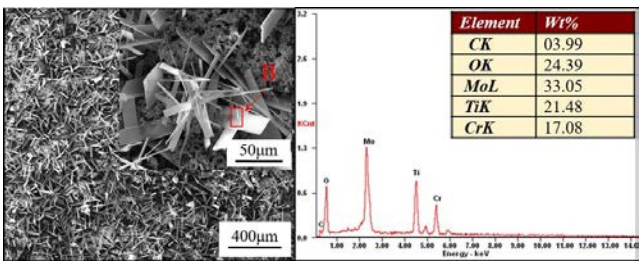

b

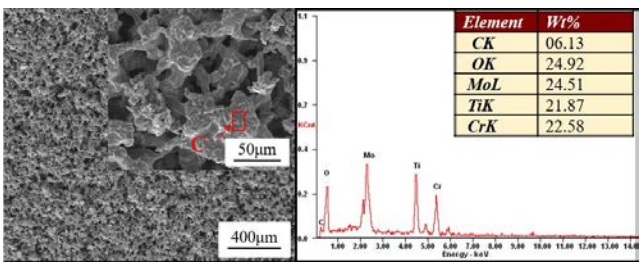

c

Fig. 3. Surface maps and EDS spectra for the Mo-TiC-Cr after oxidation: a – oxidation 10 min; b – oxidation 40 min; c – oxidation 60 min

As shown in Fig. 6 a, the surface morphology after 10 min of oxidation is mainly composed of fine particles and large flakes, with particles generally less than 1 μm in size. Considering the XRD analysis results, it can be concluded that in Fig. 3 b, the granular features are TiO_2 and the flakes are MoO_3. The distribution of the MoO_3 flakes is uneven, and the pores on the surface of the oxide layer are increased in number. The distance between the TiO_2 particles is also increased. As shown in Fig. 4 c, when the oxidation time increases to 60 min, the MoO_3 flakes completely disappear, leaving a large number of holes and interconnected but not fused granular materials on the surface. According to the XRD analysis, the oxide layer at this time is mainly Cr oxide and TiO_2 particles, both of which are connected in a granular form and exist on the surface.

Fig. 4 shows photomicrographs of the surface morphology of the Mo-TiC-xCr composites with different compositions after oxidation for 30 min. Fig. 4 shows that the surface morphology of the Mo-TiC-xCr composite material is mainly composed of fine particles and large flakes after oxidation for 30 min. According to the XRD analysis results, the particulate matter is TiO_2, and the flakes are MoO_3. The distribution of the MoO_3 flakes is uneven, the pores on the surface of the oxide layer increase, and the distance between the TiO_2 particles also increases. With a continuous increase in the Cr content, the degree of warping of the MoO_3 flakes decreases, and the TiO_2 particles also decrease. Decreasing the degree of warping of the sheet-like structure means that the porosity is reduced, and the oxidation rate of the oxygen through contact with the matrix material is also reduced, which increases the oxidation resistance of the material. This is also compatible with the results of Fig. 1. According to the XRD results, at this time, the oxide layer is mainly Cr oxide and TiO_2 particles, and both oxides are connected in the form of particles on the surface.

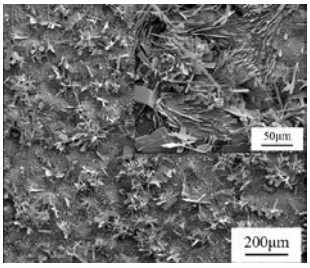

a

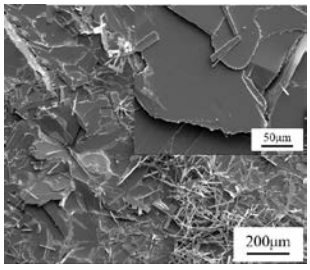

b

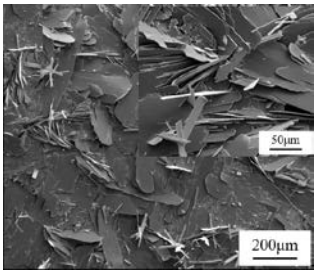

c

Fig. 4. Features of the Mo-TiC-xCr surface morphology after 30 min of oxidation: a – x = 0; b – x = 0.5; c – x = 1.0

3.4. Characteristics of the oxidation section morphology

Fig. 5 shows the backscatter photomicrographs of cross-sections of Mo-TiC-xCr composite material after oxidation for 30 min. With increasing Cr content, the average thickness of the oxide layer is 70 μm, 62 μm and 45 μm. The introduction of Cr reduces the average thickness of the oxide layer, and the thickness of the oxide layer gradually decreases with increasing Cr content. At the same time, the Mo-TiC composites contain oxide transition layers. According to related literature [23], it is known that, in general, a transition layer forms that consists of a low-quality oxide under the surface of the MoO_3, and the composition of this layer is MoO_x ($2 < x < 3$). According to the thickness of the oxide film, it is likely that as the Cr content increases, the oxidation resistance of the material is effectively improved. According to the analysis of the elements in the EDS line scan, it can be seen that the content of Mo in the oxide layer is significantly lower than that of the matrix. This is because the MoO_3 formed by the full reaction of Mo and O_2 has strong volatility and is volatile to the atmosphere through the pores [24]. The introduction of Cr suppresses this effect. With an increase in Cr, the loss of Mo in the oxide layer is effectively suppressed. In addition, the content of Ti and Cr in the oxide layer of Mo-TiC-xCr increases, and TiO_2 and Cr_2O_3 suppress the oxidation of Mo, which increases the oxidation resistance. As shown in Fig. 5 b, the content of Cr at the interface between the substrate and the oxide layer increases significantly. The analysis indicates that Cr can form a protective Cr_2O_3 oxide film between the oxide layer and the substrate.

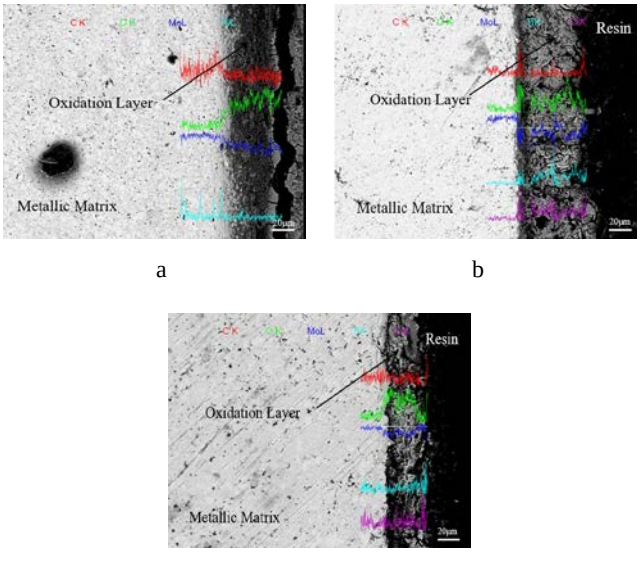

a b c

Fig. 5. Mo-TiC-xCr cross section morphology and EDS analysis results after 30 min of oxidation: a – x = 0; b – x = 0.5; c – x = 1.0

3.5. Discussion

Fig. 6 is a schematic diagram of different oxidation times of Mo-TiC-Cr composites and describes the oxidation mechanism of this material in detail. It can be seen in Fig. 6 that after sintering, the matrix in-side the material is mainly Mo, and TiC particles and part of the Mo_2C are uniformly dispersed in the Mo matrix [25]. The oxidation resistance of molybdenum is particularly low at high temperatures. It starts to oxidize when heated to approximately 300 °C in the air [26]. When the Mo-TiC-Cr alloy system is oxidized at a high temperature, the following reactions occur.

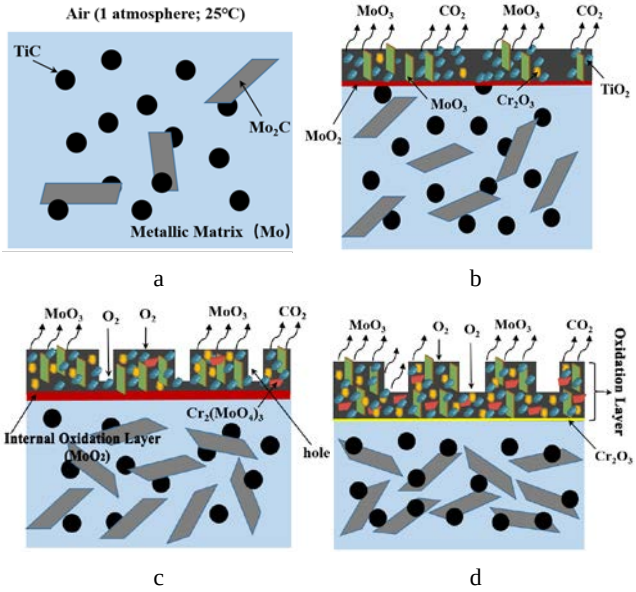

a b c d

Fig. 6. Schematic diagram of different oxidation times of Mo-TiC-Cr composites: a – oxidation 0 min; b – oxidation 10 min; c – oxidation 40 min; d – oxidation 60 min

The matrix Mo and Mo_2C produced during the sintering process react with O_2 to form MoO_2 and MoO_3, as shown in Eq. 1 – Eq. 4:

$$Mo + O_2 \rightarrow MoO_2; \quad (1)$$

$$MoO_2 + 1/2O_2 \rightarrow MoO_3; \quad (2)$$

$$Mo + 3/2O_2 \rightarrow MoO_3; \quad (3)$$

$$Mo_2C + O_2 \rightarrow 2MoO_3 + CO_2. \quad (4)$$

The dispersed TiC in the Mo matrix react with O_2 to form TiO_2, as shown in Eq. 5:

$$TiC + 2O_2 \rightarrow TiO_2 + CO_2. \quad (5)$$

The added Cr oxidizes to Cr_2O_3, and Cr_2O_3 reacts with MoO_3 to form $Cr_2(MoO_4)_3$, as shown in Eq. 6 and Eq. 7 [27]:

$$2Cr + 3/2O_2 \rightarrow Cr_2O_3; \quad (6)$$

$$Cr_2O_3 + 3MoO_3 \rightarrow Cr_2(MoO_4)_3. \quad (7)$$

During the early stage of oxidation, the surface of the molybdenum forms a dense adhesion layer comprising MoO_2. Its oxidation rate depends on the diffusion rate of the metal ions and oxygen through the oxide film [28]. The oxidation rate at this stage is slow. After the MoO_2 layer reaches a certain thickness, the MoO_2 is oxidized to MoO_3, and the formation rate of MoO_3 is equal to its evaporation rate [29]. With increasing temperature and pressure, the oxide formation and rate of volatilization are accelerated. As shown in Fig. 6 b, as the oxidation time increases, a large amount of dark green gas rises from the sample surface. This is because MoO_3 gas and CO_2 gas are generated by the reaction of two substances, Mo and Mo_2C, with oxygen. The

generated MoO_3 is volatilized and forms a dark green gas that appears in the air, so a large amount of dark green gas can be seen during the oxidation process.

After oxidation for 10 min, the surface of the oxidized sample is mainly composed of granular and lamellar structures. Combining the results in Fig. 5 and Fig. 6 a indicates that the oxidized surface is mainly composed of two kinds of oxides, namely, granular TiO_2 and MoO_3 flakes. The TiO_2 particles remain on the surface of the oxide layer, and the gas generated by the oxidation process evaporates into the air and leaves holes on the surface of the sample. A large amount of Mo and Mo_2C are oxidized violently in the air and generate a large amount of MoO_3. During the process of removing the sample from the furnace, the MoO_3 gas cannot be fully volatized. As the temperature decreases, the MoO_3 appears lamellar and remains on the oxidized surface. The evaporation of the molybdenum oxide at the oxidizing gas interface forms a porous oxide layer. These holes provide channels for oxygen to contact the substrate [30]. Due to the increased porosity, the atmosphere continues to provide O_2 through the defective outer layer. Combining the results in Fig. 5 and Fig. 6 b indicates that at this time, the number of holes increases, the area of the holes increases, and the contact area between the oxygen and the substrate increases. As the oxidation time increases, the thickness of the oxide layer further increases, and the oxidation becomes severe. The pores allow oxygen to diffuse into the matrix through a thick oxide layer, and the internal oxide layer comprising MoO_2 is violently oxidized and disappears. At this time, no oxide film is formed on the surface of molybdenum, and only the oxide is volatilized. The oxidation rate is completely determined by the volatilization process, and the speed continues to increase.

The TiC particles and Cr elements added to the Mo matrix play a crucial role in retarding the oxidation of Mo. Related studies [31] have shown that TiO_2 formed after TiC oxidation has a high melting point (1850 °C) and high temperature stability, which effectively delays the diffusion rate of oxygen to the Mo matrix, can shorten the reaction stage time, promote a stable passivation stage, and therefore improves the oxidation performance. The Cr element reacts with O_2 to form an adhesive protective oxide layer Cr_2O_3. Although Cr_2O_3 loses some antioxidation properties due to the volatilization of CrO_3 and the reaction with MoO_3 [32], the experimental results show that its protective effect is not destroyed. As the content of Cr increases, the number and thickness of Cr_2O_3 oxide layers that prevent further oxidation of the alloy also increase correspondingly, which helps to suppress oxidative corrosion. This is also consistent with the measurement results of the oxidation kinetics.

4. CONCLUSIONS

In this paper, the composition of Mo-based composites was optimized and improved, and the effect of Cr on the microstructure and properties of the material was explored. The oxidation resistance and oxidation mechanism were studied under the same oxidation temperature and different oxidation times. The conclusion is as follows: in Mo matrix composites, when the content of Cr element is less, it will hinder grain boundary movement and inhibit grain growth. When the content is high, the activation energy is reduced and the grain growth is promoted. Therefore, with the increase of Cr content, the grain size of TiC/Mo increases first and then decreases. At the same oxidation temperature, a large amount of MoO_3 flakes and TiO_2 particles were generated on the surface with increasing oxidation time. The MoO_3 flakes gradually decreased with increasing time, while the TiO_2 particles gradually increased with increasing time. The Cr oxide generated by the addition of Cr generated the protective film Cr_2O_3 and hindered the mobility of the MoO_3, which decreased the oxidation. It will be of positive significance to to design and optimization of Mo matrix composites in the application field of high-temperature structural components.

Acknowledgments

This research was Supported by Key Laboratory fund general projects (No. 6142905180203).

REFERENCES

1. **Sharna, I.G., Chakraborty, S.P., Suri, A.K.** Preparation of TZM Alloy by Aluminothermic Smelting and its Characterization *Journal of Alloys & Compounds* 393 (1 – 2) 2004: pp. 122 – 127. https://doi.org/10.1016/j.jallcom.2004.09.055
2. **Yang, J.C., Nie, Z.R.** Microstructure and Emission Ability of Rare Earth Oxides Doped Molybdenum Cathodes *Applied Surface Science* 215 (1 – 2) 2003: pp. 87 – 95. https://doi.org/10.1016/S0169-4332(03)00311-8
3. **Flem, M. L., Allemand, A., Urvoy, S., Cedat, D., Rey, C.** Microstructure and Thermal Conductivity of Mo-TiC Cermets Processed by Hot Isostatic Pressing *Journal of Nuclear Materials* 380 (1 – 3) 2018: pp. 85 – 92. https://doi.org/10.1016/j.jnucmat.2008.01.033
4. **Smolik, G.R., Petti, D.A., Schuetz, S.T.** Oxidation and Volatilization of TZM Alloy in Air *Journal of Nuclear Materials* 283 (1) 2000: pp. 1458 – 1462. https://doi.org/10.1016/S0022-3115(00)00303-2
5. **Majumdar, S., Raveendra, S., Samajdar, I., Bhargava, P., Sharma, I.G.** Densification and Grain Growth During Isothermal Sintering of Mo and Mechanically Alloyed Mo-TZM *Acta Materialia* 57 (14) 2009: pp. 4158 – 4168. https://doi.org/10.1016/j.actamat.2009.05.013
6. **Yung, D.L., Maaten, B., Antonov, M.** Oxidation of Spark Plasma Sintered ZrC-Mo and ZrC-TiC Composites *International Journal of Refractory Metals & Hard Materials* 66 2017: pp. 244 – 251. https://doi.org/10.1016/j.ijrmhm.2017.03.019
7. **Garg, P., Park, S.J., German, R.M.** Effect of Die Compaction Pressure on Densification Behavior of Molybdenum Powders *International Journal of Refractory Metals & Hard Materials* 25 (1) 2007: pp. 16 – 24. https://doi.org/10.1016/j.ijrmhm.2005.10.014
8. **Kim, G.S., Kim, H.G., Kim, D.G., Oh, S.T., Suk, M.J.** Densification Behavior of Mo Nanopowders Prepared by Mechano-Chemical Processing *Journal of Alloys and Compounds* 469 (1 – 2) 2009: pp. 401 – 405. https://doi.org/10.1016/j.jallcom.2008.01.149
9. **Brookes, K.** New Ways to Make Moly as it Enters Nano-Phase Production *Metal Powder Report* 59 (2) 2004: pp. 18 – 21. https://doi.org/10.1016/S0026-0657(04)00073-6

10. **Landwehr, S.E., Hilmas, G.E., Fahrenholtz, W.G., Talmy, I.G.** Processing of ZrC-Mo Cermets for High-Temperature Applications, Part I: Chemical Interactions in the ZrC-Mo System *Journal of the American Ceramic Society* 90 (7) 2007: pp. 1998 – 2002. https://doi.org/10.1111/j.1551-2916.2007.01667.x
11. **Ohser-Wiedemann, R., Weck, C., Martin, U., Muller, A., Seifert, H.J.** Spark Plasma Sintering of TiC Particle-Reinforced Molybdenum Composites *International Journal of Refractory Metals & Hard Materials* 32 2012: pp. 1 – 6. https://doi.org/10.1016/j.ijrmhm.2011.12.001
12. **Yung, D.L., Antonov, M., Hussainova, I.** Spark Plasma Sintered ZrC-Mo Cermets: Influence of Temperature and Compaction Pressure *Ceramics International* 42 (11) 2016: pp. 12907 – 12913. https://doi.org/10.1016/j.ceramint.2016.05.059
13. **Takida, T., Mabuchi, M., Nakamura, M., Igarashi, T., Doi, Y., Nagae, T.** Mechanical Properties of a ZrC-Dispersed Mo Alloy Processed by Mechanical Alloying and Spark Plasma Sintering *Materials Science & Engineering A* 276 (1 – 2) 2000: pp. 269 – 272. https://doi.org/10.1016/S0921-5093(99)00481-5
14. **Zhang, Z.H., Wang, F.C., Wang, L., Li, S.K.** Ultrafine-Grained Copper Prepared by Spark Plasma Sintering Process *Materials Science & Engineering A* 476 (1 – 2) 2008: pp. 201 – 205. https://doi.org/10.1016/j.msea.2007.04.107
15. **Clemow, A.J., Daniell, B.L.** Solution Treatment Behavior of Co-Cr-Mo Alloy *Journal of Biomedical Materials Research* 13 (2) 1979: pp. 265 – 279. https://doi.org/10.1002/jbm.820130208
16. **Karahan, T., Ouyang, G., Ray, P.K., Kramer, M.J.** Oxidation Mechanism of W Substituted Mo-Si-B Alloys *Intermetallics* 87 2017: pp. 38 – 44. https://doi.org/10.1016/j.intermet.2017.04.005
17. **Ray, P.K., Ye, Y.Y., Akinc, M.** Effect of Nb and W Substitutions on the Stability of the A15 Mo_3Si Phase *Journal of Alloys and Compounds* 537 2012: pp. 65 – 70. https://doi.org/10.1016/j.jallcom.2012.04.109
18. **Akinc, M., Meyer, M.K., Kramer, M.J., Thom, A.J., Huebsch, J.J., Cook, B.** Boron-Doped Molybdenum Silicides for Structural Applications *Materials Science and Engineering A* 261 (1 – 2) 1999: pp. 16 – 23. https://doi.org/10.1016/S0921-5093(98)01045-4
19. **Supatarawanich, V., Johnson, D.R., Liu, C.T.** Oxidation Behavior of Multiphase Mo-Si-B Alloys *Intermetallics* 12 (7 – 9) 2004: pp. 721 – 725. https://doi.org/10.1016/j.intermet.2004.02.011
20. **Gonzalez-Rodriguez, J.G., Rosales, I., Casales, M., Serna, S., Martinez, L.** Corrosion Performance of Molybdenum Silicides in Acid Solutions *Materials Science and Engineering A* 371 (1 – 2) 2004: pp. 217 – 221. https://doi.org/10.1016/j.msea.2003.11.041
21. **Eliaz, N., Gileadi, E.** Induced Codeposition of Alloys of Tungsten, Molybdenum and Rhenium with Transition Metals *Springer New York* 2008: pp. 191 – 301. https://doi.org/10.1007/978-0-387-49489-0_4
22. **Leonhardt, T., Carlén, J.C., Buck, M., Brinkman, C.R., Stevens, C.O.** Investigation of Mechanical Properties and Microstructure of Various Molybdenum-Rhenium Alloys *AIP Conference Proceedings* 458 (1) 1999: pp. 685. https://doi.org/10.1063/1.57638
23. **Freund, D.** Manufacture and Properties of Molybdenum-Rhenium Alloys *Metal Powder Report* 56 (6) 2001: pp. 39 – 39. https://doi.org/10.1016/S0026-0657(01)80366-0
24. **Agnew, S.R., Keene, J.I., Dong, L., Shamsujjoha, M.** Microstructure Characterization of Large TiC-Mo-Ni Cermet Tiles *International Journal of Refractory Metals & Hard Materials* 68 2017: pp. 84 – 95. https://doi.org/10.1016/j.ijrmhm.2017.07.004
25. **Compton, B.G., Zok, F.W.** Impact Resistance of TiC-Based Cermets *International Journal of Impact Engineering* 62 2013: pp. 75 – 87. https://doi.org/10.1016/j.ijimpeng.2013.06.008
26. **Yadroitsev, I., Bertrand, P., Smurov, I.** Parametric Analysis of the Selective Laser Melting Process *Applied Surface Science* 253 (19) 2007: pp. 8064 – 8069. https://doi.org/10.1016/j.apsusc.2007.02.088
27. **Al Mangour, B., Grzesiak, D.** Selective Laser Melting of TiC Reinforced 316L Stainless Steel Matrix Nanocomposites: Influence of Starting TiC Particle Size and Volume Content *Materials & Design* 104 2016: pp. 141 – 151. https://doi.org/10.1016/j.matdes.2016.05.018
28. **Li, B., Wang, J., Chen, X., Li, R., Zhang, G.J.** High-Temperature Oxidation Response of Mo-Si-B Composites with TiO2w /SiCw Addition *Ceramics International* 45 (13) 2019: pp. 16046 – 16053. https://doi.org/10.1016/j.ceramint.2019.05.120
29. **Floquet, N., Bertrand, O., Heizmann, J.J.** Structural and Morphological Studies of the Growth of MoO_3 Scales During High-Temperature Oxidation of Molybdenum *Oxidation of Metals* 37 (3) 1992: pp. 253 – 280. https://doi.org/10.1007/BF00665191
30. **Dong, B.L., Simkovich, G.** Oxidation of Molybdenum-Tungsten-Chromium-Silicon Alloys *Oxidation of Metals* 31 (3 – 4) 1989: pp. 265 – 274. https://doi.org/10.1007/BF00846689
31. **Grabke, H.J., Meier, G.H.** Accelerated Oxidation, Internal Oxidation, Intergranular Oxidation, and Pesting of Intermetallic Compounds *Oxidation of Metals* 44 (1 – 2) 1995: pp. 147 – 176. https://doi.org/10.1007/BF01046726
32. **Paul, B., Koley, S., Suri, A.K.** A Novel Approach to Determine Oxidation Kinetics of Mo–16Cr–xSi (x = 4-6 wt.%) Alloy Using Stepwise Isothermal Thermo-Gravimetry *Thermochimica Acta* 549 2012: pp. 57 – 62. https://doi.org/10.1016/j.tca.2012.09.018